

Header styling inspired by CS 70: <https://www.eecs70.org/>.

### Abstract

In this lab, we investigate electronic transitions between the  $|F, m_F\rangle \rightarrow |F, m_F + 1\rangle$  energy levels using a method called "optical pumping", which is achieved by using a circularly polarized light source to excite electrons, and a radio-frequency (RF) magnetic field. We used two isotopes of rubidium,  $^{85}\text{Rb}$  and  $^{87}\text{Rb}$ , and measured their resonances to experimentally confirm the Breit-Rabi formula in a weak field. Then, using linear fits to the experimental data, we calculated the nuclear spins of both isotopes, and also calculated Earth's magnetic field. These values were then compared to accepted values to verify the accuracy of our experiment.

## 1 Introduction

This report concerns the OPT experiment in the Physics 111B Experimentation Laboratory. In this report, we will begin by detailing the theoretical background for the phenomena, then analyze the data we collect to verify our theoretical results.

## 2 Background

In this experiment, the primary phenomenon we investigate is the transition of electrons between different quantum states, which are split due to perturbations in the environment. To motivate where this splitting comes from, consider the quantum state of a hydrogen (or hydrogen-like) atom that is unperturbed:

$$\psi_{n\ell m}(r, \theta, \phi) = R_{n\ell}(r, \theta)Y_{\ell m}(\theta, \phi)$$

where  $R_{n\ell}(r, \theta)$  and  $Y_{\ell m}(\theta, \phi)$  are the radial and spherical harmonic functions, respectively. As such, there are limits on the values of  $n, \ell$  and  $m$ . In particular, we have  $\ell \in \{0, \dots, n - 1\}$  and  $m \in \{-\ell, \dots, \ell\}$ . The associated energies with these states are given by the Bohr formula:

$$E_n = - \left[ \frac{m_e}{2\hbar^2} \left( \frac{e^2}{4\pi\epsilon_0} \right)^2 \right] \frac{1}{n^2} = \frac{E_1}{n^2}$$

The crucial thing to note in this equation is that the associated energy depends only on  $n$ , which is important because this means that there is degeneracy in our system: different values of  $\ell$  and  $m$  don't change the energy of the system, and imply that there is symmetry among these values. This symmetry is important, as we will explore in the next section.

### 2.1 Perturbation Theory

In perturbation theory, we are particularly interested in how small changes in our Hamiltonian affect the eigenstates of the unperturbed Hamiltonian. In general, these perturbations are regarded as changes which disturb the symmetry of a particular parameter in our wavefunction, which manifests as changes in observables associated with that parameter. In the sections below we will explore two perturbations, both of which will break the symmetry we initially had above.

#### 2.1.1 The Fine Structure Perturbation

The fine structure perturbation is actually comprised of two different perturbations, which we will consider in combination. The first is the relativistic perturbation, which we need to consider because the electron moves at relativistic speeds, and the second is the spin orbit coupling, which is an interaction between the electron spin and the surrounding magnetic field produced by moving charges.

Since the relativistic perturbation only changes the effective kinetic energy and linear momentum of the electron, the perturbation is symmetric with respect to the angular terms  $\ell$  and  $m$ . It is not symmetric with respect to  $n$ , since  $n$  determines the total energy of the system, which is affected in this case. As a result, only  $E_n$  is perturbed, and the new energies are now:<sup>1</sup>

$$E_r = -\frac{E_n^2}{2mc^2} \left[ \frac{4n}{\ell + 1/2} + 3 \right]$$

The spin-orbit coupling is a more interesting perturbation. To explain its origin, consider the hydrogen atom from an electron's perspective. To the electron, the proton is orbiting around it, and this moving charge generates a magnetic field which interacts with the intrinsic spin of the electron. In particular, the energy of an electron which is aligned with the magnetic field has lower energy than one which is anti-aligned, and thus this interaction breaks the symmetry we initially had in  $\ell$  and  $m$ . From the principles of perturbation theory, we know that to find the energy corrections we need to find "good states" of the Hamiltonian (i.e. quantum numbers whose associated operators commute with the perturbation  $H'$ ), and we find that in this case that would be the total angular momentum  $\mathbf{J} = \mathbf{L} + \mathbf{S}$ . That is, the degeneracy (symmetry) in  $j$  is broken, so now different values of  $j$  have different energies. The spin correction is of the form:

$$E_{\text{so}} = \frac{E_n^2}{mc^2} \left[ \frac{n(j(j+1) - \ell(\ell+1) - 3/4)}{\ell(\ell+2)(\ell+1)} \right]$$

Combining this with the relativistic correction from earlier, we derive the fine structure correction:

$$E_{\text{fs}} = \frac{E_n^2}{2mc^2} \left( 3 - \frac{4n}{j + 1/2} \right)$$

Here,  $E_n$  represents the uncorrected energy levels of Hydrogen, as defined earlier.

### 2.1.2 The Zeeman Effect

So far, we've looked at perturbations which intrinsically exist in the system. That is, these weren't perturbations that result from external sources, but rather corrections which we now consider because we want to be more precise about the exact energy levels of Hydrogen. Now, we turn to the Zeeman effect, which are the corrections to the energies when the atom is placed in a uniform external magnetic field  $\mathbf{B}_{\text{ext}}$ . Intuitively, one can think of this perturbation as one which breaks the symmetry in  $m$ , since the energy of the electron changes depending on whether the spin is aligned or anti-aligned with this external magnetic field.

The energy correction formulas depend on the strength of the field  $\mathbf{B}_{\text{ext}}$ . In our experiment, we won't really be dealing with strong magnetic fields, so we will be working in the weak field regime. Here, we consider  $H_Z$  (the Zeeman correction) as the perturbation, and the unperturbed Hamiltonian is  $H_{\text{Bohr}} + H_{\text{fs}}$  combined. Working out the perturbation theory, we find that the energy corrections are given by:

$$E_Z = \mu_B g_J B_{\text{ext}} m_j$$

Here,  $m_j$  is the total spin angular momentum of the system. In reality, only the electron spin is varying, so the only allowed values for  $m_j = \pm \frac{1}{2}$ , depending on the spin of the electron.

Although this derivation allows us to pretty easily arrive at the energy corrections, we could have also done a similar derivation using a "coupled basis", in which we express the states according to their total angular momentum, denoted by  $\mathbf{F} = \mathbf{J} + \mathbf{I}$ .<sup>2</sup> In this notation, the states are labeled  $|J, I, F, m_F\rangle$ , where  $m_F$  is the projection of  $\mathbf{F}$  onto the  $z$ -axis. This will be useful later on, since it allows us to characterize state transitions in a cleaner way. We can also write out the mathematical formula for the correction  $E_Z$  in this new basis, but for this it's more useful to look at a graph of the energy corrections, which are provided to us by [2], in figure 1:

---

<sup>1</sup>The reason  $\ell$  appears in this equation is just a result of calculating expectation values for  $\langle \frac{1}{r^2} \rangle$ , which has an  $\ell$  term. It does not mean that the symmetry in  $\ell$  has broken.

<sup>2</sup>This really is just the same as  $\mathbf{J}$ , since  $\mathbf{I}$  is constant, but we will use this notation because this was what was used in the lab manual [1].

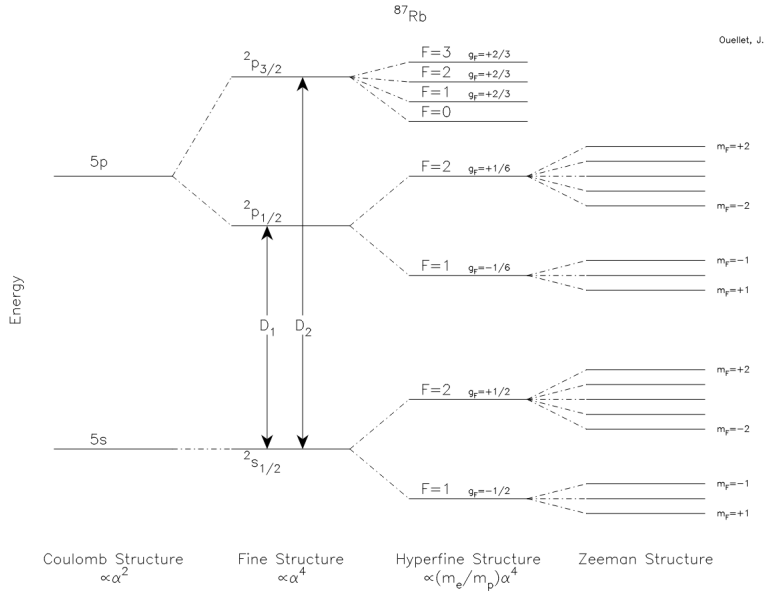


Figure 1: Diagram showing the energy splitting due to the Zeeman effect, provided to us by [2].

### 2.1.3 The Breit-Rabi Formula

The Breit-Rabi formula gives a relationship between the resonant frequency of an atom and its relationship between it and the external magnetic field applied  $\mathbf{B}_{\text{ext}}$ . Written, it is expressed as:

$$\frac{\nu}{\mathbf{B}_{\text{ext}}} = \frac{2.799}{2I+1} \frac{\text{MHz}}{\text{G}} \quad (1)$$

Here,  $\nu$  is the resonant frequency and  $I$  is the nuclear spin. The derivation for this equation is rather long and involves using ladder operators  $L_+$  and  $L_-$ , so we won't go into it in extreme detail here. For further information, see the appendix.

## 2.2 Optical Pumping

With the perturbation theory out of the way, we now turn to the some theoretical aspects of the experiment that we should become familiar with. To begin, the objective for our experiment is to measure the transitions between two quantum states  $|F, m_F\rangle$  and  $|F, m_F \pm 1\rangle$  in an atom. However, the probability of an atom existing in either of these two states is actually equal, which we can see in the following equation:

$$\frac{P_2}{P_1} = \exp\left(-\frac{E_2 - E_1}{k_B T}\right)$$

This is because the distribution of energies follows a Boltzmann distribution, and the states  $|F, m_F\rangle$  and  $|F, m_F \pm 1\rangle$  have the same energy. Thus, in order for us to see a transition, we need to alter this probability somehow. This is the method which we call *optical pumping*. Optical pumping involves sending in polarized light, which changes this distribution by causing the electrons in the atom to excite, giving the transition  $|F, m_F\rangle \rightarrow |F, m_F + 1\rangle$ . Then, the electron emits infrared light, and changes  $m_F$  by  $\Delta m_F = \{-1, 0, 1\}$  with equal probability. Because the excitation step only increases the quantum number, then over many iterations we will find that the value  $m_F$  tends to increase, and thus we will eventually get all the atoms in the state with the highest energy, which, in the case of a magnetic field in the  $z$  direction, corresponds to the highest possible  $m_F$ . This is not true in general of course – if the magnetic field direction were flipped, then the lowest value of  $m_F$  would be the highest energy state. This highest energy state is also called the *pumped state*, which is the term I will be using to describe it in the rest of this report.

In the highest  $m_F$  state, the electrons cannot absorb any more light, since the absorption requires that we increase  $m_F$  by one. As a result, when the atoms reach this state, they become unable to absorb the polarized light, and are considered to be in a "dark" state. In order to bring them out of this state, we drive the atoms with a radio frequency (RF) magnetic field, which has the effect

of driving the atoms out of the pumped state, into states which can absorb more light. We can detect such changes through the use of a photodetector positioned directly to measure the amount of light that passes through the atoms – if the atom is not in the dark state, then the electrons will absorb the light we feed it and the photodetector will read a low light level, whereas in the dark state since no light is absorbed the photodetector will read a high light level. With this setup, we are now able to detect the required atomic transitions.

### 3 Experimental Setup

A diagram of the experimental setup used is shown in figure 2. The main component of our experimental setup is the small glass bulb in the middle, which sits in an insulating metal box. This glass bulb contains our  $^{85}\text{Rb}$  and  $^{87}\text{Rb}$  atoms, along with an inert gas. At room temperature, the rubidium atoms exist as a solid which coats the walls of the glass. This is not ideal, and instead we want some of the rubidium atoms to exist as a gas, so to achieve this we heat the bulb to a temperature such that some of the rubidium atoms would be promoted to a gaseous state. This heating is achieved through a resistive heating element, controlled by the heating control unit. A thermometer is placed inside the insulating box to so we can monitor the temperature in the bulb, allowing us to keep the temperature approximately constant throughout the experiment.

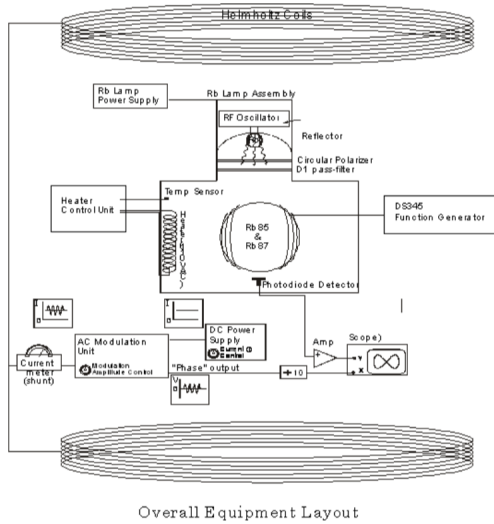


Figure 2: Block diagram of the experimental setup with labeled components, provided by [1].

Surrounding the bulb are two metal coils which connect to a DS345 function generator. These coils are responsible for generating the RF magnetic field that drives pumped atoms out of the aforementioned "dark state", back into a state where they can absorb polarized light. Next, we have a lamp assembly at the top of the box, whose light is sent through a circular polarizer to keep only the circularly polarized portions of the light. The light that goes through the gas is then captured by the photodiode at the bottom of the box, after it passes through the rubidium gas. The signal from the photodiode also tends to be small (since only a small amount of rubidium atoms actually release into the gas), so we pass the signal through a signal amplifier before it is fed into the oscilloscope.

Finally, the last component of our experimental setup is are the large Helmholtz coils that surround the thermally insulating box. The coils are connected to an alternating current source, which is the source of our magnetic field  $\mathbf{B}_{\text{ext}}$  that generates the Zeeman effect. The coil has  $N = 135$  turns and a radius  $a = 27.5$  cm, parameters that will become important when we calculate  $\mathbf{B}_{\text{ext}}$ . The current is measured through a current meter (shunt), which tells us the strength of the magnetic field we are using. The phase is also output through a separate channel; its use will be clear in the next section.

## 4 Experimental Procedure

In this section, we detail the experimental procedures we carried out during this experiment. Due to the multitude of measurements we will be taking, this section will be broken down into subsections, under which the specific procedure for each section is detailed. There are some common steps we took with each measurement, which we will detail in the following paragraph.

First, we would turn on all the relevant electronic devices (scopes, function generators, etc.), and begin by using the temperature controller to heat the insulating box containing the rubidium to a temperature around 53°C, then we would turn off the heating element, as it produces a magnetic field strong enough to interfere with our measurements. The heating element would remain off until the temperature got below 40°C, after which we would restart the heater until the temperature rose 53°C again. Along with the procedure, some preliminary background calculations will be made; these are quantities that are not data but information given to us, so we will calculate them here.

### 4.1 Observation of ODMR

The objective of this section is to experimentally confirm that the optical pumping procedure "works", as intended, and we can experimentally verify the presence of the Zeeman splitting and resonance. To do this, we will use the large Helmholtz coils, and pass a fixed DC current through it. When we pass a DC current through the coils, it generates a magnetic field, which due to the coil separation and overall geometry, can be approximated as a constant magnetic field – that is, the vector  $\mathbf{B}$  field is a constant vector between the coils. With this approximation in hand, we can derive a formula for the strength of the magnetic field (this comes from basic electrodynamics):

$$B = \frac{32\pi NI}{5\sqrt{5}a} \times 10^{-7} \text{ Tesla} = \frac{32\pi NI}{5\sqrt{5}a} \times 10^{-3} \text{ Gauss} \quad (2)$$

For this section, we are instructed to keep the current at  $I = 1 \text{ A}$ , so with  $N = 135$  turns and  $a = 27.5 \text{ cm}$ , we are able to conclude that the strength of the magnetic field at  $I = 1 \text{ A}$  is:

$$\mathbf{B}_{\text{ext}} = 4.41 \times 10^{-4} \text{ T} = 4.41 \text{ G}$$

Recall that 1 Gauss = 1000 Tesla. Now, with this knowledge, we can calculate the resonant frequencies of  $^{85}\text{Rb}$  and  $^{87}\text{Rb}$  using the Breit-Rabi formula from earlier, substituting this value of  $\mathbf{B}_{\text{ext}}$  in. So, we get:

$$\nu_{\text{Rb}85} \approx 2.059 \text{ MHz} \quad \nu_{\text{Rb}87} \approx 3.087 \text{ MHz}$$

To verify these ODMR resonances, we first heat up the chamber, then set the DS345 function generator to sweep over sine waves of a defined frequency range. The sweep also has an associated sweep period, a parameter which also needs to be carefully tuned to see the ODMR peaks. To see why, consider a sweep over the frequencies between 2-3 MHz. This covers both the resonance peaks calculated above, so we should see two peaks in the sweep. However, these peaks would only be present if there were atoms in the  $m_F = 0$  state which had the ability to excite (recall that the atoms reside in the "dark state" until they are down pumped), meaning that if the sweep had been too fast, we would get fewer atoms in the  $m_F = 0$  state, and as such this would lead to a shallower peak in the resonance measurement. While conducting the experiment, we found that a sweep period of  $T = 1 \text{ s}$  worked out the best, but unfortunately because it was so slow we couldn't really get a good picture of both peaks showing up on the oscilloscope. That said, we do confirm that we saw two resonance peaks, similar to those shown in figure 3. Finally, the last measurement we took in this step was to approximately determine the resonance frequencies of  $^{85}\text{Rb}$  and  $^{87}\text{Rb}$ . To do this, we gradually narrowed down the frequency sweep range so that the left edge of the sweep would be as close to the resonant frequency as possible; this was obviously repeated for both isotopes. These measurements were intentionally crude, mainly because more precise measurements would be made later in the lab anyway, so this measurement serves only as an approximate guide so we know in which frequency range we should expect to see each peak. From these measurements, we found that the resonances for  $^{85}\text{Rb}$  and  $^{87}\text{Rb}$  were approximately 1.9 MHz and 2.8 MHz, respectively.

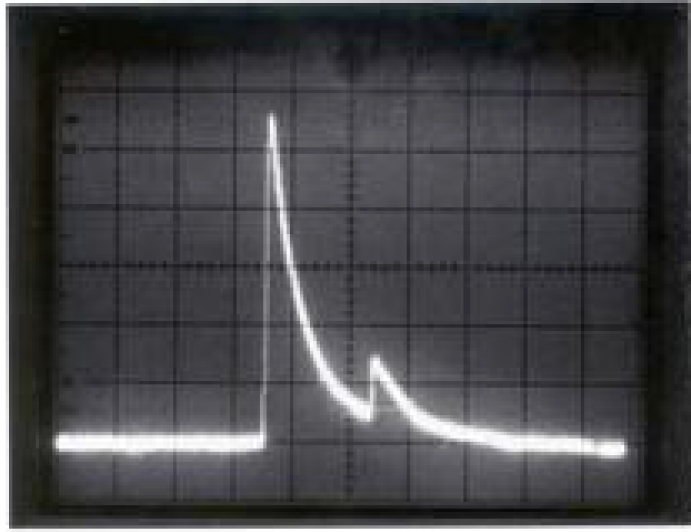


Figure 3: ODMR peaks on the oscilloscope when sweeping over an appropriate frequency range. This image was taken from [1], because we could not get a good image showing the entire sweep range as an image.

## 4.2 Good settings for bulb temperature

In this section, the objective was to determine the optimal temperature of the bulb for our measurements. That is, because the experimental apparatus is inherently temperature dependent, our objective was to find the ideal temperature for our measurements such that we see the maximum resonance. To do this, we first heat the chamber to around 52°C, and continue to do the frequency sweep outlined in the previous section, with the sweep range narrowed down so that we see only one of the two peaks. This temperature was chosen because it was as close to 55°C as we were comfortable in approaching, as the lab manual instructed us to not exceed this temperature. Then, as the temperature decreased over time, we recorded the temperature and also the amplitude of the resonant peak. This measurement was done by eye, by counting the height of the peak using the number of grid lines the peak passes through. We did this over a temperature range from approximately 42°C to 52°C, and the dependence on temperature we obtained is given in table 1, and a scatter plot of this relationship is shown in figure 4a. For the errors in our measurements here, we are confident in counting the number of grid lines up to 0.3 of a grid<sup>3</sup>, which is also displayed on the plot.

As is evident in the plot, we found that while there are small changes in the amplitude of the peak, the changes are not very significant over the span of the entire temperature range we took data in. While this does not replicate the plot that was given to us in [1] (figure 4b), this is not incredibly alarming however, because not only is figure 4b a plot of an entirely different experiment, but these results really just tell us that any measurements between 42°C to 51°C should be significant enough that they are detectable, and we don't need to be incredibly specific about the temperature we take the data at.

That said, it would certainly have been nicer to demonstrate that the temperature range of approximately 40°C to 50°C was an *ideal* range to take our data in rather than an acceptable range, but this would require us to have taken more data below 40°C, which we did not do.

## 4.3 Lock-in detection of the Resonance Frequency

For this section, the objective is to carry out a more precise measurement of the resonance frequency, as we outlined earlier how the approach of determining the resonance through sweeping was incredibly imprecise (not to mention also very tedious as well). Instead, a more precise method of determining the resonance frequency would be to find the current needed through Helmholtz coils to produce resonance, while holding the RF pumping at a specific frequency. The reason this is because the down-pumping step is very sensitive to frequency variations, so even if the down-pumping frequency were slightly off there would be very few

---

<sup>3</sup>this is relatively generous, but it is much preferred to overestimate than to underestimate the error.

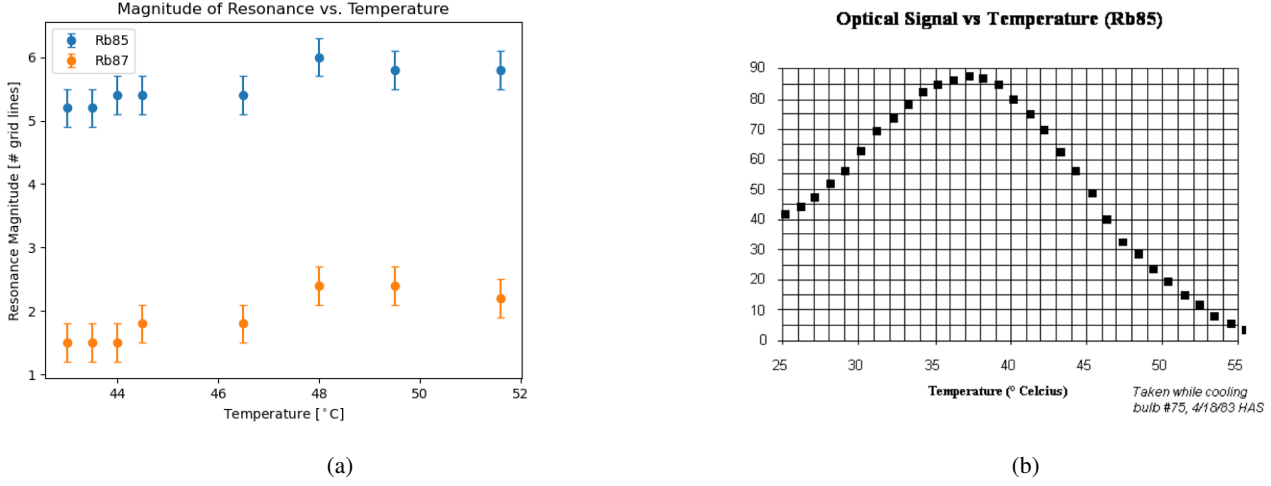


Figure 4: (a) Measured resonance magnitude and its relationship to temperature. Note that while we do observe the peak resonance at approximately  $48^{\circ}\text{C}$ , we do find that the variation across the entire temperature range is not significant enough for it to drastically impact our measurements. (b) A plot of the same experiment, provided to us by [1].

atoms which successfully pump down. This provides us with far greater accuracy over our measurements than the sweep strategy we had earlier, for obvious reasons.

In addition to this, we also introduce a "lock-in" method for detection, which involves sending an AM modulated signal to the Helmholtz coils instead of DC. There are two main reasons we do this: firstly, the modulation allows us to send in an AC signal, which allows us to reduce the noise in the system, as there aren't many noise sources at high frequency when compared to low frequency. Second, this AC modulation also allows us to sweep over the Zeeman resonance many times per second in a single cycle of the envelope wave, effectively giving us more measurement data.<sup>4</sup> Plotting the modulated current signal on the  $x$ -axis of the scope and the photodiode signal on the  $y$ -axis, we see what is called a *Lissajous curve* on the scope screen, as shown in figure 5.

At resonance, we should see an equal spike in the photodiode signal on both the positive and negative edge of the modulated current, due to symmetry. On the scope, this manifests itself as a *symmetric Lissajous curve* along the  $y$ -axis. That is, the intersection of the Lissajous curve onto itself occurs on the vertical axis, which is exactly what is depicted in figure 5. In order to capture such a shape, we first set the RF function generator to some frequency around the previously captured resonant frequency, then vary the modulated current until we observe a symmetric signal on the scope. Then, to determine the uncertainty bounds on our measurements, we continue varying the current, and record the current values at which the Lissajous curve becomes clearly asymmetric. In terms of the data we took, we captured data for 7 different RF frequencies, for both isotopes, and each RF frequency was captured twice: once for forward and reverse polarity, the latter of which was achieved by simply reversing the direction of the current.

#### 4.4 Zero-Field Resonance

In this section, we tune the Helmholtz coils to generate a magnetic field that exactly cancels Earth's magnetic field, placing the box in what is effectively a "zero field". Then, we vary the current exactly as before to find a symmetric Lissajous curve. The strength of the magnetic field is calculated using our measurements from the previous part.

#### 4.5 Timescale of Pumping

In this section, the objective is to determine the characteristic time it takes for all the atoms to enter and leave the pumped state. To do this, we use the RF function generator to send a sinusoid signal modulated by a square envelope, and plot the photodiode

<sup>4</sup>Even though this isn't data we directly collect, these extra passes through the data really help us in determining the resonance peaks.

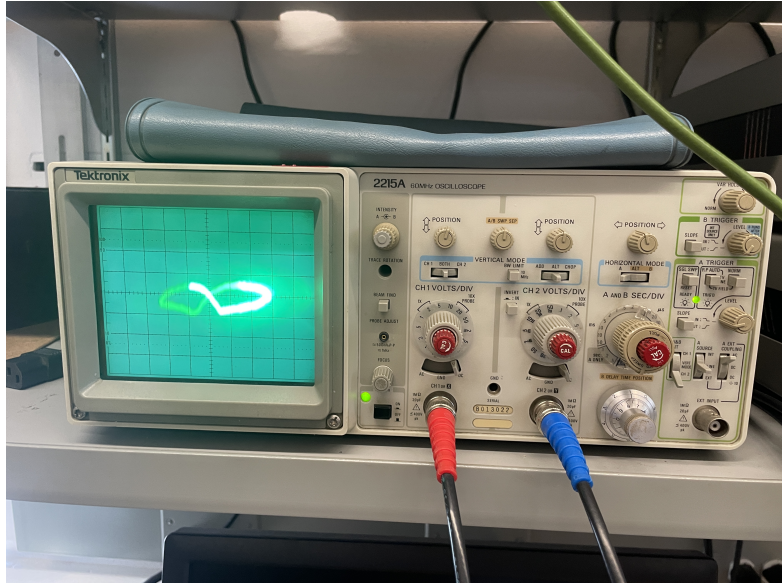


Figure 5: Centered Lissajous curve on the oscilloscope screen. On the  $x$ -axis is the modulated current signal, the  $y$ -axis is the photodiode signal. Note that the intersection of the Lissajous curve onto itself is exactly on the  $y$ -axis, which is what we define to be "centered".

signal over time. Then, we can record the signal on video, and determine the characteristic time by analysing the frames in the video. In order to maximize the accuracy of our measurement, this last step was done in a video editing software, in which it is possible to go through the video frame by frame.

## 5 Analysis

### 5.1 Resonance Frequency vs. Current

The data we took for both isotopes is provided in table 11a and table 11b. The first portion of the analysis will be dedicated to experiment 4.3, where the objective is to experimentally verify the Breit-Rabi formula (equation 1). For convenience, the Breit-Rabi formula is reiterated below:

$$\frac{\nu}{\mathbf{B}_{\text{ext}}} = \frac{2.799}{2I+1} \frac{\text{MHz}}{\text{G}}$$

This  $\mathbf{B}_{\text{ext}}$  is the total magnetic field, so we need to split it into  $\mathbf{B}_{\text{coil}} + \mathbf{B}_{\text{ambient}}$ , where  $\mathbf{B}_{\text{coil}}$  is the magnetic field generated by the large Helmholtz coils, and  $\mathbf{B}_{\text{ambient}}$  is the ambient magnetic field at Berkeley. Moving this  $\mathbf{B}$  term to the right hand side, we get the following equation:

$$\nu = \frac{2.799}{2I+1} (\mathbf{B}_{\text{coil}} + \mathbf{B}_{\text{ambient}})$$

In terms of the quantities we measure, we have resonant frequency  $\nu$  and also the magnetic field generated by the coil  $\mathbf{B}_{\text{coil}}$ , so this equation suggests a linear fit between  $\nu$  and  $\mathbf{B}_{\text{coil}}$ . The ambient magnetic field is dominated by Earth's magnetic field at Berkeley, which we can obtain from [3] to be  $\mathbf{B}_{\text{ambient}} = 47645.9 \text{ nT}$ . One thing to note is that in our plots, we will be plotting the current on the  $y$ -axis, so in this case we actually need to rearrange this equation to solve for  $\mathbf{B}_{\text{coil}}$ , which gives us the following equation:

$$\mathbf{B}_{\text{coil}} = \frac{2I+1}{2.799} \nu - \mathbf{B}_{\text{ambient}} \quad (3)$$

Then, substituting in the formula we have  $\mathbf{B}_{\text{coil}}$  in terms of the current, we will have our expected slope and  $y$ -intercept. This will be done later, after we have seen the plots. For now, we will move on to the scatter plot and the fits.

The scatterplot of the data and an unweighted least squares fit can be found in figure 6. As can be seen in the plots we fit the data to a linear function of  $y = mx + b$ , and use `scipy.optimize.curve_fit()` to perform a least-squares fit on the data. As

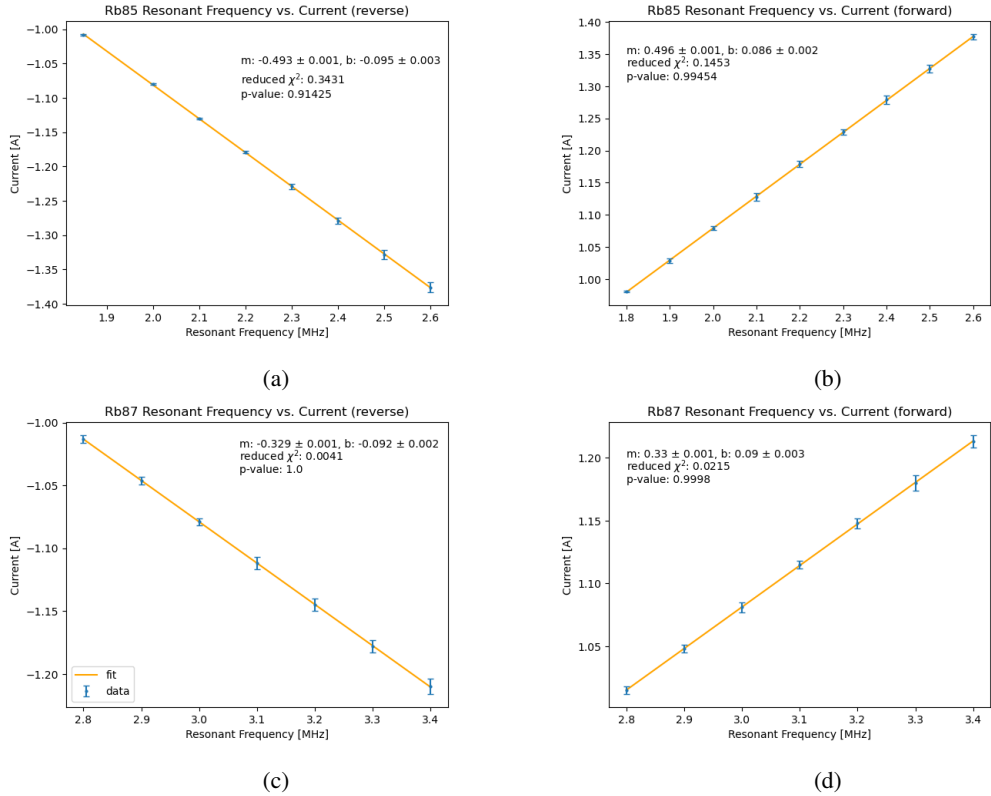


Figure 6: Resonant frequency vs. Current for  $^{85}\text{Rb}$  and  $^{87}\text{Rb}$ , for both forward and reverse polarities, computed using an unweighted linear fit. Statistical quantities such as  $\chi^2$  and  $p$ -values are also calculated for each fit, and are displayed in their respective plots.

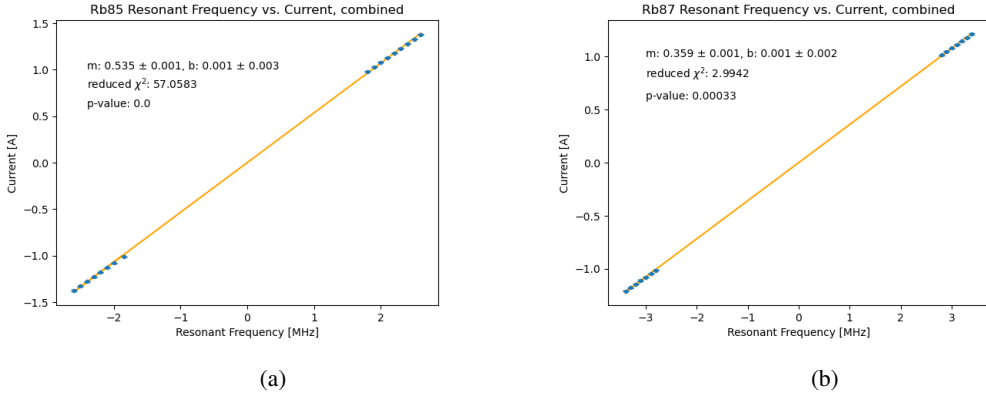


Figure 7: Resonant frequency vs. Current for  $^{85}\text{Rb}$  and  $^{87}\text{Rb}$  for both current polarities combined, computed using an unweighted least-squares fit. Statistical quantities such as  $\chi^2$  and  $p$ -values are also calculated for each fit.

can be seen in the plots, the reduced  $\chi^2$  values for all the plots are less than 2, which is considered a good fit according to [4]. Their associated  $p$ -values also suggest that our null hypothesis (in this case, the linear fit) is to be trusted, which confirms the linear relationship we expect as predicted by equation 1. One additional plot we can generate using this data is to plot the positive and negative polarities together. To do this, all we have to do is flip the resonance frequencies for the polarities to a *negative* frequency; physically a negative frequency doesn't really make much sense, but one way to think about this is in the same way negative momentum is interpreted: as a wave moving in the opposite direction.

Figure 7 shows the least-squares fit when both polarities are combined. Unlike the individual plots, we find that the  $p$ -value of this plot is 0, which indicates to us that the errors in this plot are statistically significant enough that our null hypothesis (our linear fit) should be rejected. In addition, the reduced  $\chi^2$  values for both these plots are too large ([4] gives  $\chi^2 \geq 1.5$  as the threshold) so this statistic also indicates that our fit is not to be trusted. This is to be expected, since it makes no sense to have a current associated with a resonance frequency when we set the function generator to output a DC signal; the down-pumping requires a signal whose frequency is equal to that of the energy gap from the Zeeman splitting, and such an energy is not achievable with a DC signal. As a result, we can't really determine the relationship around  $\nu = 0$ .

With that said, the reason the  $p$ -values are so low is largely due to the extremely small uncertainties we have on our fitted values of  $m$  and  $b$  from the individual plots in figure 6. That is, taking a look at the  $^{85}\text{Rb}$  individual plot, our values of  $m$  and  $b$  lie around  $m = 0.49 \pm 0.001$ ,  $b = 0.09 \pm 0.002$  (these values are intentionally crude; there's not much reason to be precise here, we'll see why in a moment), whereas the fitted values for the combined plot in 7 is  $m = 0.535 \pm 0.001$ ,  $b = 0.001 \pm 0.003$ . Comparing the two values and their reported uncertainties, it's easy to see that they fall well outside of each other, up to many times the standard deviation. This would be the case even if we had been more precise with how we obtained a combined  $m$  and  $b$ , since the uncertainties are just so small. As a result, the  $p$ -value for these two events simultaneously occurring is exceedingly low, which is why the combined plot gives us a  $p$ -value of zero.

In addition to an unweighted least-squares fit, we can also compute a weighted fit, using the same method we described in the EAX. Doing so, we obtain the plots shown in figures 8 and 9. Using the weighted fit, we can see that our  $p$ -values are much higher, the  $\chi^2$  values are still below our threshold of  $\chi^2 \leq 2$ , which combine to again give us evidence that a linear fit is appropriate here. Despite incorporating the weights into our fit, this still doesn't really help our combined plots, which still have  $p$ -values near zero.

Comparing the fitted values of  $m$ ,  $b$  between the weighted and unweighted fit, taking the negative polarity data  $^{85}\text{Rb}$  as an example, we have the following:

	unweighted	weighted
$m$	$-0.493 \pm 0.01$	$-0.49 \pm 0.002$
$b$	$-0.095 \pm 0.03$	$-0.101 \pm 0.004$

We can see that the weighted and unweighted fits agree relatively well. This is to be expected, because based on our raw data,

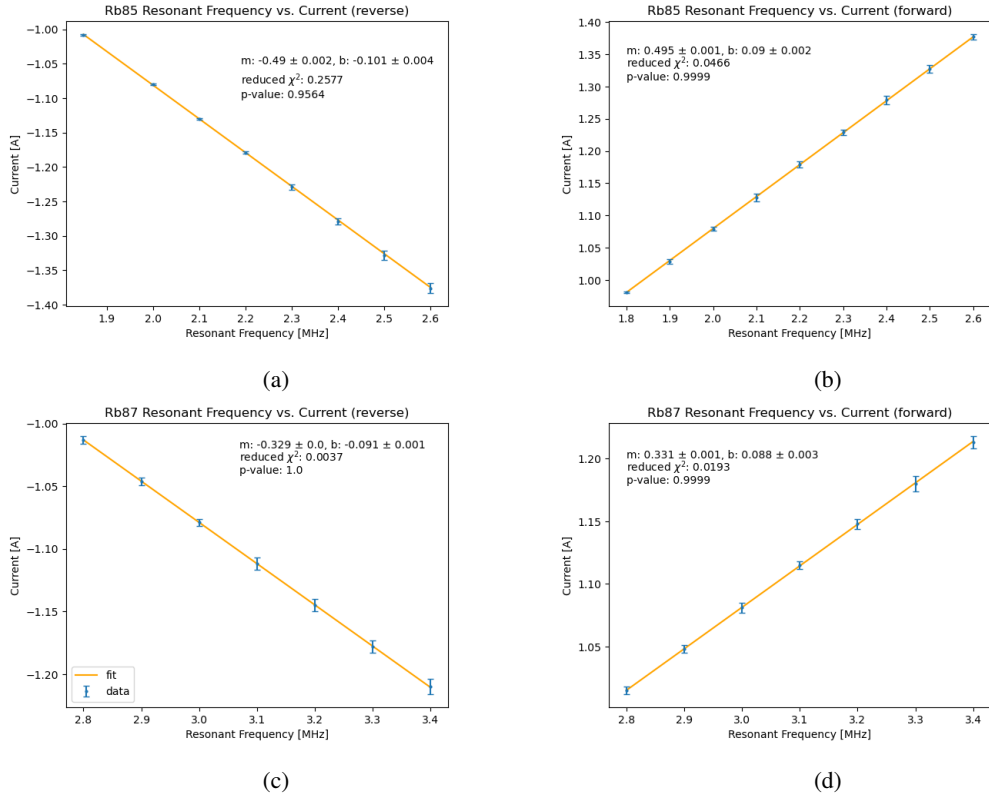


Figure 8: Resonant frequency vs. Current for  $^{85}\text{Rb}$  and  $^{87}\text{Rb}$ , for both forward and reverse polarities, computed using a weighted linear fit. Statistical quantities such as  $\chi^2$  and  $p$ -values are also calculated for each fit, and are displayed in their respective plots.

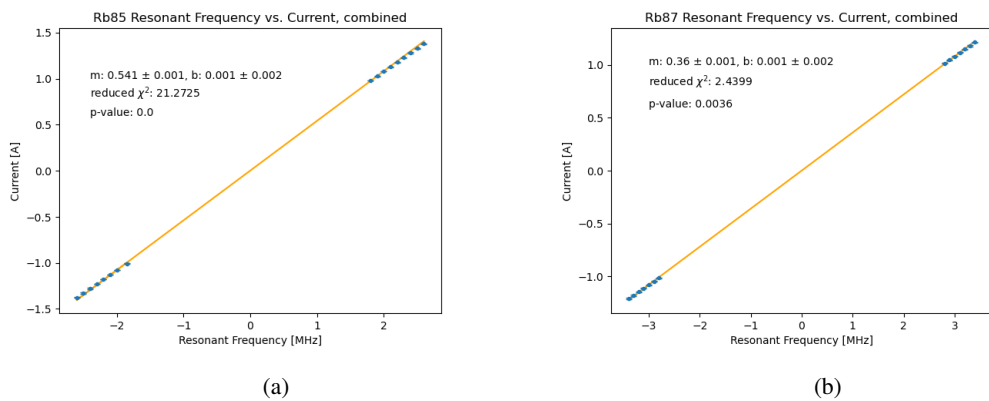


Figure 9: Resonant frequency vs. Current for  $^{85}\text{Rb}$  and  $^{87}\text{Rb}$  for both current polarities combined, computed using a weighted least-squares fit. Statistical quantities such as  $\chi^2$  and  $p$ -values are also calculated for each fit.

it is clear that there isn't any glaring outlier that we would like to weight less, which is precisely what a weighted least-squares fit attempts to mitigate against. Then, by this logic, every data point should be treated with equal weight, so therefore we will proceed with an unweighted least-squares fit for the rest of the analysis.

## 5.2 Determination of Nuclear Spins

### 5.2.1 Approach I

With the linear fits completed, the next thing we can determine is the nuclear spins of the rubidium atoms, which we can do by looking at the fit parameters. In particular, if we examine equation 3 combine what we have from 2, we get the following relation:

$$i = \frac{5\sqrt{5}a}{32\pi N} \cdot 10^3 \left( \frac{2I+1}{2.799} \nu + \mathbf{B}_{\text{ambient}} \right) = \frac{1}{\alpha} \left( \frac{2I+1}{2.799} \nu - \mathbf{B}_{\text{ambient}} \right) \quad (4)$$

where  $i$  is the current, and  $\alpha = \frac{32\pi N}{5\sqrt{5}a} \cdot 10^3$ . From this, we can extract the slope by looking at the prefactor of  $\nu$ , and then ultimately solving for  $I$ :

$$m = \frac{1}{\alpha} \frac{2I+1}{2.799} \implies I = \frac{\alpha m \cdot 2.799 - 1}{2}$$

here  $m$  is the slope of the fit. The associated error is then given by:

$$\delta_I = \sqrt{\delta_\alpha^2 \left( \frac{2.799m}{2} \right)^2 + \delta_m^2 \left( \frac{2.799\alpha}{2} \right)^2} \quad (5)$$

However, in our case, we claim that  $\delta_\alpha$  is actually zero, because there is no uncertainty in  $N$  (obviously), and there isn't any uncertainty reported in  $a = 27.5$  cm, so we will treat it as an exact value. Thus, only the  $\delta_m$  term survives. For our experimental value of  $m$ , we will take the arithmetic mean of both current polarities for each isotope. If  $m_1, m_2$  are the positive and negative polarity slopes and  $\delta_{m_1}, \delta_{m_2}$  are their respective uncertainties, then we know that the errors add in quadrature:

$$\delta_{\bar{m}} = \sqrt{\delta_{m_1}^2 \left( \frac{1}{2} \right)^2 + \delta_{m_2}^2 \left( \frac{1}{2} \right)^2}$$

So, this leaves us with the following slopes:

$$\bar{m}_{\text{Rb85}} = 0.494 \pm 0.0079 \quad \bar{m}_{\text{Rb87}} = 0.329 \pm 0.00059$$

Note that the numbers are rounded in the report for simplicity, but they are kept exact during all calculations. Using these reported average slopes and their uncertainties, putting them into equation 5, we get:

$$I_{\text{Rb85}} = 2.5557 \pm 0.0048 \quad I_{\text{Rb87}} = 1.5363 \pm 0.0036$$

These values are incredibly close to the accepted values for nuclear spin,  $I_{\text{Rb85}} = 5/2$  and  $I_{\text{Rb87}} = 3/2$ . This confirmation between the experimental and the theoretical values for the nuclear spin shows strong evidence that we are observing the exact phenomena we were looking for – the electron transitions between different Zeeman levels.

### 5.2.2 Approach II

An alternative approach we can use to determine nuclear spins is to examine the ratios of the resonant frequencies for  $^{85}\text{Rb}$  and  $^{87}\text{Rb}$ . To do this, we return to the original Breit-Rabi formula from equation 1:

$$\frac{\nu}{\mathbf{B}_{\text{ext}}} = \frac{2.799}{2I+1}$$

Now, if we measure  $\nu$  for each isotope at the same intensity of  $\mathbf{B}_{\text{ext}}$ , then we can divide the two together to get a ratio of the resonant frequencies for the same magnetic field strength:

$$\frac{\nu_{85}}{\nu_{87}} = \frac{2I_{87}+1}{2I_{85}+1} = \frac{2}{3}$$

In this equation, because we did not record any uncertainties for our frequency values, we unfortunately won't be able to perform error propagation on this equation. Further, because we controlled the current instead of the resonant frequency, we cannot guarantee that we have the same strength of  $\mathbf{B}_{\text{ext}}$  for any of the data points; to remedy this, we will instead make use of the average linear fits we obtained in the previous section to get the resonant frequencies for a given current value for both isotopes. The errors in these values we can then propagate to find an "average error" of the resonance frequency ratio.

To be a more specific in how we computed this value, we first chose a common range of currents, and sampled 20 points within this range. Then, from our linear fit, we used the following equations to calculate the corresponding resonance frequency and its error:

$$x = \frac{-b + y}{m}, \quad \delta_x = \sqrt{\delta_b^2 \left(-\frac{1}{m}\right)^2 + \delta_m^2 \left(\frac{b - y}{m}\right)^2}$$

We repeat this for both the  $^{85}\text{Rb}$  and  $^{87}\text{Rb}$  samples, and then compute the ratio and its corresponding error:

$$\text{ratio} = \frac{\nu_{85}}{\nu_{87}}, \quad \delta_{\text{ratio}} = \sqrt{\delta_{85}^2 \left(\frac{1}{\nu_{87}}\right)^2 + \delta_{87}^2 \left(-\frac{\nu_{85}}{\nu_{87}}\right)^2}$$

then as a final step, we take the average of both the ratio and its uncertainty to generate a final report for our experimentally calculated nuclear spin ratio. Doing so for the positive and negative polarities separately, we get ratios of  $0.66659 \pm 0.032$  for the positive and  $0.66624 \pm 0.030$  for the negative polarity. These two values both agree very well with the predicted value of  $\frac{2}{3} = 0.6$ , so this calculation gives us further agreement between the data and our theory, and also verifies that our previous calculations for  $I_{85}$  and  $I_{87}$  agree well with our theory.

### 5.3 Accuracy of Helmholtz Coils

The next thing we are asked to determine is to take a look at the accuracy of the Helmholtz coils, by picking a value of positive and negative polarity, and use our determined value for the nuclear spins to solve for the strength of  $\mathbf{B}$ . We use the same coil for  $^{85}\text{Rb}$  and  $^{87}\text{Rb}$ , so picking one positive and negative current is enough – no need to pick two separately for the two isotopes. So, we choose the resonance at  $\nu = 1.85$  MHz for the negative polarity and  $\nu = 1.8$  MHz for the positive. Using equation 3, we get:<sup>5</sup>

$$\mathbf{B}_{\text{coil, negative}} = 3.563 \pm 0.059 \text{ G} \quad \mathbf{B}_{\text{coil, positive}} = 3.454 \pm 0.059 \text{ G}$$

Calculating this using equation 2 using the measured current, we get:

$$\mathbf{B}_{\text{coil, negative}} = 4.44 \pm 0.021 \text{ G} \quad \mathbf{B}_{\text{coil, positive}} = 4.33 \pm 0.021 \text{ G}$$

we can see that the predicted magnetic field strength is vastly different than what we should theoretically be getting from the Helmholtz coils. This difference is more than statistically significant, but at the same time this is to be expected, especially considering that the equipment in this lab is at least twice my age. Furthermore, there are also other sources of error, such as our limited accuracy on the Bohr magneton  $\mu_B$ , though this source of error, while existent, is not very likely to be the source of this discrepancy because the gap is simply too large for a better  $\mu_B$  to dramatically improve the agreement.

### 5.4 Ambient Magnetic Field

Finally, the last thing we can calculate using this data is the ambient magnetic field strength. This quantity is contained in the  $y$ -intercept of the data, since according to equation 4, we have

$$b = \frac{\mathbf{B}_{\text{ambient}}}{\alpha}$$

We also computed an average  $y$ -intercept which we calculated in section 5.2.2, so we can just use that value to determine  $\mathbf{B}_{\text{ambient}}$ . Using this, we get:

$$\mathbf{B}_{\text{ambient, Rb85}} = 0.401 \pm 0.0078 \text{ G} \quad \mathbf{B}_{\text{ambient, Rb87}} = 0.402 \pm 0.0080 \text{ G}$$

---

<sup>5</sup>I am still doing the error propagation, but I do feel like I've written it out enough times that it's clear I know how to do it; from here on out I won't keep writing it.

Compared to the ambient magnetic field at Berkeley given by [3] of  $\mathbf{B}_{\text{ambient}} = 0.476459$  G, this is relatively close, but our uncertainties are still too small to conclude that our calculated ambient magnetic field strength matches third-party data. Some possible sources for this discrepancy could be also due to the discrepancy in the strength of the Helmholtz coils – after all, the discrepancy in the coil strength is a large systematic error, the absence of which could very well lead to a better calculation of  $\mathbf{B}_{\text{ambient}}$ . That said, with all things considered this value is still close enough that personally, I'd call this a relative success.

## 5.5 Zero Field Measurement

The only unfortunate thing about our lab report is that we could not get the zero-field resonance to work properly. We aren't particularly sure what was the cause of this issue either; we did ask for assistance and none of the GSIs who helped us (including the professor) could figure it out. In principle, we could find the current required – this would just be our  $y$ -intercept, since it's the current value which corresponds to a resonant frequency of 0, or in other words the point when the degeneracy in the Zeeman levels is restored, indicative of zero field. Therefore, we can just report our average  $b$ -value we got from the previous section as our current:  $i = 0.09 \pm 0.001$  A. However, we have nothing to experimentally check this against, because we failed to collect the requisite data for this section. That said, we did hear from the GSIs that the value for this current should be very small so there is a chance this value is possibly close to the experimental value, but there's just no way for us to know.

## 5.6 Characteristic Pumping Time

The final to analyze is the characteristic time for the pumping and de-pumping steps. To do this, we took a video of the photodiode signal over time while sending in a square modulated wave, and count the amount of time elapsed between the jumps. This process was completed using video editing software for the maximum accuracy (see figure 10). That said, we still won't have errors in the traditional sense, because the video editing software (Adobe Premiere Pro) counts the number of frames as a discrete number, so there is no uncertainty. The data from this counting is given in table table 2, and computing the mean and standard deviation, we get:<sup>6</sup>

$$\begin{array}{ll} t_{\text{Rb85, up}} = 0.113 \pm 0.0053 \text{ s} & t_{\text{Rb87, up}} = 0.113 \pm 0.010 \text{ s} \\ t_{\text{Rb85, down}} = 0.125 \pm 0.013 \text{ s} & t_{\text{Rb87, down}} = 0.113 \pm 0.0053 \text{ s} \end{array}$$

Due to the limited number of data points we took in this section, it's hard to be extremely confident in these statistics, but one good check here is that the two isotopes have the same characteristic time, which we do expect. The time it takes to pump the gas is also very close to the time it takes to de-pump, and this correspondence also gives credibility to our data, as this is also a phenomenon we expect. Overall, despite having more data points to sample, we do find that the data is consistent with our theory.

## 6 Reflection & Conclusion

Overall, our experimental data. and the results derived from them matched our expected theoretical results very well. We found a good correspondence between our linear fits and the data, both visually and also by comparing the slope and  $y$ -intercept to what we expect them to be numerically. We further confirmed the linear relationship we expect by experimentally calculating the individual nuclear spins for  $^{85}\text{Rb}$  and  $^{87}\text{Rb}$  in two different ways. In both methods, we get a remarkably good agreement between the experimental and theoretical values, which is strong evidence to support the fact that we are observing the expected Zeeman transitions.

We then also calculated the ambient magnetic field, and comparing it to the ambient magnetic field at Berkeley, provided to us by [3], we find a relatively good agreement there as well (despite them not agreeing fully).

Our experiment isn't all full of successes, however. One major issue we ran into, and manifested itself as the lack of data for the zero field measurement, is the fact that we did not fully understand what we were doing before doing it. As a result, we spent way more time on certain sections than we really should have, and this resulted in us not having enough time to fully work out the

---

<sup>6</sup>We have to convert the frame data into seconds. The video was shot at 30 fps, so we can extrapolate the time duration of each from there.

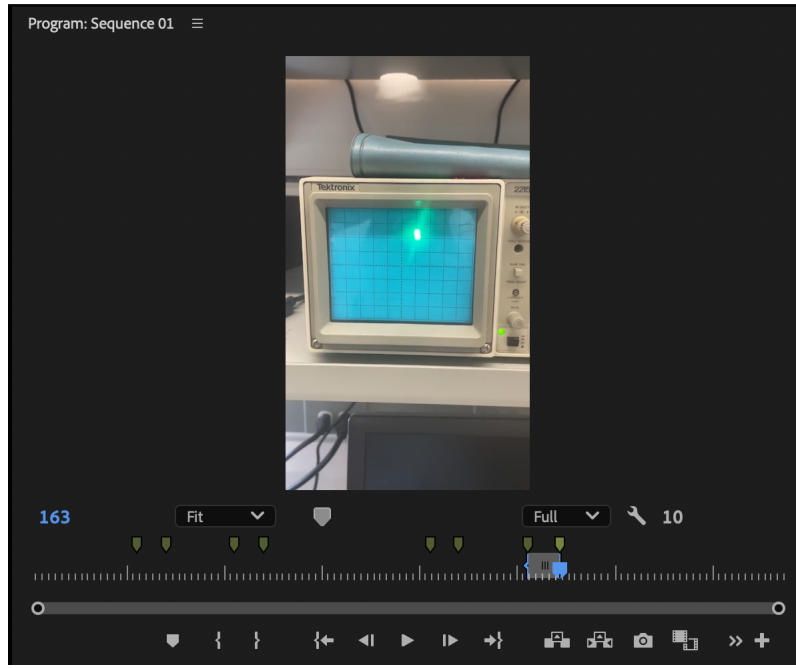


Figure 10: Screenshot of Adobe Premiere Pro, the software which was used to determine the characteristic time. This screenshot was taken when measuring the pumping time for  $^{85}\text{Rb}$ ; the green markers show the start and end of the pumping and the gray patch on the rail shows the window during which the sample is being pumped. The gray number on the right denotes how many frames have elapsed.

zero field measurement. This is also manifested in the resonance vs. current data, since there are some frequency values where we only have the current data for one of the two polarities – we initially did not establish a standard for which frequencies we would be using, and also did not have time at the end to go back and collect more data. Luckily, this did not affect our results very much, but there is easily a world where this does impact our experiment greatly and we walk away without good data to analyze. Overall, this experiment was very fun and interactive: being able to tune the current until we see the effects of phenomena that we predicted all the way back in 137B (I took this a year and a half ago now) is incredibly satisfying, and shows that quantum mechanics does work!

## References

- [1] Physics 111B: Advanced Experimentation Laboratory. *Optical Pumping*. URL: [http://experimentationlab.berkeley.edu/sites/default/files/writeups/OPT\\_Manual\\_2024-01-08.pdf](http://experimentationlab.berkeley.edu/sites/default/files/writeups/OPT_Manual_2024-01-08.pdf).
- [2] Jonathan Ouellet. *Energy Levels for Rb*. Nov. 13, 2010.
- [3] *World Magnetic Model*. Version 2020. May 14, 2020. doi: [10.25921/11v3-da71](https://doi.org/10.25921/11v3-da71). URL: <https://www.ngdc.noaa.gov/mgg/geoportal/rest/metadata/item/gov.noaa.ngdc%3AWMM2020/html> (visited on 10/26/2024).
- [4] Ifan Hughes and Thomas Hase. *Measurements and Their Uncertainties: A Practical Guide to Modern Error Analysis*.

## A Raw Data

### A.1 Finding good settings for Bulb temperature

Temperature ( $\pm 0.1$ )	Resonant Frequency	
	Rb85 ( $\pm 0.3$ )	Rb87 ( $\pm 0.3$ )
51.6	5.8	2.2
49.5	5.8	2.4
48.0	6.0	2.4
46.5	5.4	1.8
44.5	5.4	1.8
44.0	5.4	1.5
43.5	5.2	1.5
43.0	5.2	1.5

Table 1: Temperature vs. Amplitude of resonance. The uncertainty in our data is the same for all data points, so the uncertainty is listed at the top of the table.

## A.2 Resonance Frequency vs. Current

Resonance Frequency (MHz)	Current (A)	
	Forward Polarity	Reverse Polarity
1.8		$-1.008 \pm 0.001$
1.85	$0.981 \pm 0.001$	
1.9	$1.029 \pm 0.004$	
2	$1.079 \pm 0.003$	
2.1	$1.128 \pm 0.006$	
2.2	$1.179 \pm 0.005$	
2.3	$1.229 \pm 0.004$	
2.4	$1.279 \pm 0.007$	
2.5	$1.327 \pm 0.006$	
2.6	$1.377 \pm 0.004$	

Resonance Frequency (MHz)	Current (A)	
	Forward Polarity	Reverse Polarity
2.8	$1.015 \pm 0.003$	$1.013 \pm 0.003$
2.9	$1.048 \pm 0.003$	$1.046 \pm 0.003$
3.0	$1.081 \pm 0.004$	$1.079 \pm 0.003$
3.1	$1.115 \pm 0.003$	$1.112 \pm 0.005$
3.2	$1.148 \pm 0.004$	$1.145 \pm 0.005$
3.3	$1.180 \pm 0.006$	$1.178 \pm 0.005$
3.4	$1.213 \pm 0.005$	$1.210 \pm 0.006$

(a)

(b)

Figure 11: Resonant Frequency vs. Current for both (a)  $^{85}\text{Rb}$  and (b)  $^{87}\text{Rb}$ . Note that while taking data for the  $^{85}\text{Rb}$  dataset, we made a mistake and took the current for  $\nu = 1.8$  MHz for reverse polarity only, and we took  $\nu = 1.9$  MHz for the forward polarity only.

### A.3 Characteristic Time

Rb85		Rb87	
$t_{\text{up}}$	$t_{\text{down}}$	$t_{\text{up}}$	$t_{\text{down}}$
9	12	10	10
9	10	8	10
9	10	10	10
10	9	9	9

Table 2: Characteristic time for the non-pumped gas to become pumped ( $t_{\text{up}}$ ) and the down-pumping time ( $t_{\text{down}}$ ) for both isotopes. This number is reported in frames, which is an exact quantity, so for that reason there are no uncertainties.